

STAR-RIS Aided NOMA in Multi-Cell Networks: A General Analytical Framework with Gamma Distributed Channel Modeling

Ziyi Xie, *Student Member, IEEE*, Wenqiang Yi, *Member, IEEE*,
 Xuanli Wu, *Member, IEEE*, Yuanwei Liu, *Senior Member, IEEE*, and
 Arumugam Nallanathan, *Fellow, IEEE*

Abstract

The simultaneously transmitting and reflecting reconfigurable intelligent surface (STAR-RIS) is capable of providing full-space coverage of smart radio environments. This work investigates STAR-RIS aided downlink non-orthogonal multiple access (NOMA) multi-cell networks, where the energy of incident signals at STAR-RISs is split into two portions for transmitting and reflecting. We first propose a fitting method to model the distribution of composite small-scale fading power as the tractable Gamma distribution. Then, a unified analytical framework based on stochastic geometry is provided to capture the random locations of RIS-RISs, base stations (BSs), and user equipments (UEs). Based on this framework, we derive the coverage probability and ergodic rate of both the typical UE and the connected UE. In particular, we obtain closed-form expressions of the coverage probability in interference-limited scenarios. We also deduce theoretical expressions in traditional RIS aided networks for comparison. The analytical results show that there exist optimal energy splitting coefficients of STAR-RISs to simultaneously maximize the system coverage and ergodic rate. The numerical results demonstrate that: 1) RISs enhance the system coverage and NOMA schemes help improve the rate performance; 2) in low signal-to-noise ratio (SNR) regions, STAR-RISs outperform traditional RISs while in high SNR regions the conclusion is opposite.

Z. Xie and X. Wu are with the School of Electronics and Information Engineering, Harbin Institute of Technology, Harbin 150001, China (email: {ziyi.xie, xlwu2002}@hit.edu.cn).

W. Yi, Y. Liu, and A. Nallanathan are with the School of Electronic Engineering and Computer Science, Queen Mary University of London, E1 4NS, U.K. (email: {w.yi, yuanwei.liu, a.nallanathan}@qmul.ac.uk).

Index Terms

Multi-cell networks, non-orthogonal multiple access, reconfigurable intelligent surface, simultaneous transmission and reflection, stochastic geometry

I. INTRODUCTION

Requirements for high data rates and heterogeneous services in future sixth-generation (6G) wireless networks bring challenges to system designs [1]–[3]. The smart radio environment (SRE) is envisioned to be a promising solution [3], [4]. Equipped with several low-cost reconfigurable elements and a smart controller, a reconfigurable intelligent surface (RIS) is capable of intelligently altering the phase and even the amplitude of signals [5], [6], hence the propagation of which is controllable and the SRE can be realized. However, the main issue of traditional reflecting-only RISs in existing works is that user equipment (UE) can only receive reflected signals from base stations (BSs) located at the same side of the assisted RIS, which may degrade the coverage performance especially for those blocked UEs. Thanks to the recent development of metasurfaces, the concept of simultaneous transmitting and reflecting RISs (STAR-RISs) has been proposed, where incident signals can not only be reflected within the same half-space in front of the RIS, but can be refracted to the other half-space [7]–[9]. Thus, STAR-RISs are able to provide full-space coverage of SRE.

As stated in [7], there are three practical operating protocols for STAR-RISs, namely energy splitting (ES), mode switching (MS), and time switching. In ES and MS protocols, since the incident signal is split into two portions by the STAR-RIS, a multiple access scheme is required to distinguish these two parts for successful demodulation at different target UEs. Compared with orthogonal multiple access (OMA), non-orthogonal multiple access (NOMA) has been considered to be a competent technique due to its ability for the spectral efficiency enhancement and UE fairness guarantee [10]–[12]. The key idea of the NOMA scheme is to serve multiple UEs in the same resource block (RB) by employing superposition coding and successive interference cancellation (SIC) at transmitters and receivers, respectively. On the other hand, the deployment of STAR-RISs is beneficial to NOMA systems. For NOMA UEs with weak channel conditions, STAR-RISs are able to create stronger transmission links. Moreover, since STAR-RISs have the capability of adjusting channel gains of different NOMA UEs, they can offer flexible decoding orders according to the priority of UEs.

A. Related Works

For RIS aided networks, initial research contributions have paid attention to the performance analysis in single-cell systems. In these works, the channel modeling for RIS assisted communications are firstly investigated as it plays an important role when theoretically evaluating the enhancements and limitations of RISs. The authors in [13] derived the far-field path loss expression based on physical optics techniques and pointed out that the path loss value is correlated to the product of two distances of the cascaded link. In [14], the authors obtained free-space path loss in both near-field and far-field cases. Experimental measurements were also carried out to validate the accuracy of the analysis results. Considering the small-scale fading, most existing works utilized approximations to characterize the composite channel gain, where RISs are regarded as integrated antennas [15]–[18]. The authors in [15] and [16] assumed that the number of RIS elements is sufficiently large, and hence the central limit theorem (CLT) was applied to approximate the distribution of the channel gain. After that, the system capacity and the spatial throughput were derived in [15] and [16], respectively. For arbitrary number of elements, the authors in [17] and [18] employed the convolution theorem to evaluate the asymptotic outage probability in STAR-RIS aided networks. A curve fitting method was also proposed in [18]. Different from the above works, the authors in [19] derived the exact coverage probability using Gil-Pelaez inversion, where Nakagami- m fading was considered.

Recently, the system performance of RIS aided multi-cell networks has been evaluated. In [20], the authors employed a RIS at the edge of two cells to mitigate severe co-channel interference. The authors in [21] considered a multi-cell multiple-input single-output network, where transmit and reflective beamforming vectors were jointly optimized to maximize the minimum weighted signal-to-interference-plus-noise ratio (SINR) at UEs. For large-scale deployment scenarios, system optimizations were investigated in [22] and [23]. In [22], the optimal association solution among BS, RIS, and UE was obtained for maximizing the utility of the considered system. In [23], the authors focused on the capacity improvement in a cell-free structure. These works optimized the system parameters in particular setups with fixed BSs and RISs. To characterize the randomness property of large-scale networks, stochastic geometry is an efficient tool, which has been widely utilized to evaluate the average performance of multi-cell networks with largely deployed RISs [24]–[26]. However, in this scenario, channel models proposed in single-cell setup

have to be further simplified to tractable formats. A recent work [24] considered double-Rayleigh fading and approximated the composite channel gain as the Gamma distribution. Besides, based on a tractable linear RIS model proposed in [27], the authors in [25] and [26] analyzed the coverage probability and rate performance.

Motivated by the benefits including high spectral efficiency and the flexible SIC order from the integration of RISs and NOMA, recent research efforts have been devoted to RIS-enabled NOMA systems. System optimizations were considered in [28]–[31]. The authors in [28] maximized the area of the cell coverage by optimizing RIS placement. In [29], the authors proposed a joint design to maximize the achievable system sum rate. Multiple parameters including beamforming vectors and power allocation coefficients were jointly optimized for the total transmit power minimization in [30] and [31]. By leveraging stochastic geometry, the spatial effects of large-scale RIS deployment were evaluated in both single-cell networks [32] and multi-cell networks [25], [26]. Additionally, the authors in [33] investigated the performance enhancement of coordinated multipoint transmissions in a two-cell setup. However, all these works adopted traditional reflecting-only RISs, and the research on STAR-RIS aided NOMA networks is scarce. In STAR-RIS enhanced NOMA transmissions, optimization problems focused on sum rate maximization [34] and optimality gap minimization [35] were considered. For theoretical analysis, a recent work [18] first evaluated three STAR-RIS operating protocols in a NOMA single-cell network.

B. Motivations and Contributions

As we have discussed previously, NOMA schemes are able to enhance the spectral efficiency for STAR-RISs aided networks, while STAR-RISs have the potential to offer full-space coverage as well as decoding flexibility for NOMA systems. Although some initial works have validated the enhancement of STAR-RISs, most of them focused on specific small-scale fading environments, and the theoretical analysis in large-scale deployment scenarios has not been considered yet. Therefore, in this work, we first provide a tractable and accurate expression to characterize the composite channel model with general small-scale fading. In order to shed light on the performance improvement brought by STAR-RISs in multi-cell networks, a stochastic geometry-based analytical framework for a general case is then proposed. The main contributions are summarized as follows:

- We derive a general expression to characterize the distribution of the small-scale fading power of the composite channel including multiple independent RIS-based channels. By exploiting the CLT and the method of moment, the channel power gain (CPG) can be approximated by the Gamma distribution, whose parameters are only related to the mean value and the variance of the considered small-scale fading model. Additionally, a simple asymptotic expression is obtained for the case with a large number of RIS elements N . Due to the channel hardening effect, the asymptotic value of CPG for the STAR-RIS aided link is a constant when $N \rightarrow \infty$.
- Considering downlink transmissions, we propose an analytical framework for the STAR-RIS aided NOMA multi-cell networks based on stochastic geometry, where the distributions of BSs, STAR-RISs, and UEs are independent homogeneous Poisson point processes (PPPs). In this framework, STAR-RISs are employed to assist the blocked typical UE in paired NOMA UEs to communicate with its BS, while the connected UE directly associates to the BS. By limiting the locations of BSs within the same half-space of the typical UE, this framework can be applied in the traditional RIS aided networks.
- Focusing on the ES protocol, we evaluate the coverage performance and ergodic rate for this STAR-RIS aided networks. Using a novel analytical method, we derive the theoretical expressions of these two metrics for both the typical UE and the connected UE. In particular, the interference-limited case is considered as a special case, where we obtain closed-form expressions for the coverage probability. We also provide expressions in traditional RIS aided networks for comparison. Besides, the impact of the energy splitting coefficients is investigated. The analytical results demonstrate that the system performance can be improved by adjusting the energy splitting coefficients.
- The numerical results validate our theoretical analysis and illustrate that: 1) The employment of two kinds of RISs significantly enhances the coverage performance of NOMA systems; 2) in low signal-to-noise ratio (SNR) regions, STAR-RISs with appropriate energy splitting coefficients outperform traditional RISs, while in high SNR regions the conclusion is opposite; 3) STAR-RISs bring flexibility to NOMA systems by reconfigurable energy splitting coefficients.

C. Organizations

The rest of this paper is organized as follows. In Section II, we introduce the system model of the STAR-RIS aided NOMA multi-cell networks that we consider. In Section III, we provide a fitting method to characterize the small-scale fading for general cases. In section IV, we derive the analytical expressions of the coverage probability. In Section V, we derive the analytical expressions of the ergodic rate. Section VI presents numerical results. Finally, we draw the conclusions in Section VII.

II. SYSTEM MODEL

In this paper, STAR-RIS aided downlink NOMA multi-cell networks are considered. The locations of BSs, STAR-RISs, and UEs obey three independent homogeneous PPPs Φ_B , Φ_R , and Φ_U in \mathbb{R}^2 with density λ_B , λ_R , and λ_U . Both BSs and UEs are equipped with a single antenna. The transmit power of BSs is P_B . The STAR-RIS consists of N reflecting elements, all of which are able to simultaneously transmit and reflect signals. To improve the spectral efficiency, two NOMA UEs are grouped in each orthogonal RB in this work. We define a UE randomly selected from Φ_U as the typical UE. The location of the typical UE is fixed at the origin of the considered plane. Without loss of generality, we assume that the other one of the paired UEs has been connected to the tagged BS, which joints the same RB of the typical UE to form the typical NOMA pair.

A. Channel Model

There are two types of communication links between the target BS and a UE u_0 in this networks: the direct link and the transmissive/reflective link created by STAR-RISs. The detailed descriptions of both links are provided in the following.

The channel model of the direct communication link is similar to that in conventional cellular networks, which is formulated as a Rayleigh fading channel. The overall channel between the BS $i \in \Phi_B$ and the UE u_0 can be expressed as

$$H_{0,i} = \sqrt{C_d d_{0,i}^{-\alpha_d}} h_d, \quad (1)$$

where $L_{0,i} = C_d d_{0,i}^{-\alpha_d}$ is the path loss for the direct link. The C_d is the intercept. The α_d is the path loss exponent. The $d_{0,i}$ represents the distance between the BS and the UE. The h_d is the small-scale fading and obeys Rayleigh distribution.

For the STAR-RIS aided link, since the STAR-RISs is regarded as integrated antennas in this work, there are N communication channels between the BS i and the UE u_0 . We denote $\Theta^\chi = \sqrt{\beta^\chi} \text{diag}(e^{j\theta_1^\chi}, e^{j\theta_2^\chi}, \dots, e^{j\theta_N^\chi})$ as the transmissive/reflctive-coefficient matrix of the STAR-RIS, where the notation χ represents the transmission mode for the signal, i.e., $\chi = T$ and $\chi = R$ represent transmitting and reflecting signals, respectively. In particular, $j = \sqrt{-1}$, $\theta_n^\chi \in [0, 2\pi)$ with $n \in \{1, 2, \dots, N\}$, $\beta^\chi \in [0, 1]$ is the energy splitting coefficient. As the STAR-RISs are passive and the other energy consumption is assumed to be ignorable, we have $\beta^T + \beta^R = 1$. We also denote the small-scale fading vectors of the BS-RIS link and the RIS-UE link as $\mathbf{H}_{BR} = [h_{BR,1}, h_{BR,2}, \dots, h_{BR,N}] \in \mathbb{C}^{N \times 1}$ and $\mathbf{H}_{RU} = [h_{RU,1}, h_{RU,2}, \dots, h_{RU,N}] \in \mathbb{C}^{N \times 1}$, respectively. The overall channel gain from the BS i to the UE u_0 assisted by the STAR-RIS $k \in \Phi_R$ can be expressed as

$$H_{0,i}^{(k)} = \sqrt{C_r \left(r_i^{(k)} d_0^{(k)} \right)^{-\alpha_r}} (\mathbf{H}_{RU})^H \Theta^\chi \mathbf{H}_{BR}, \quad (2)$$

where $L_{0,i}^{(k)} = C_r \left(r_i^{(k)} d_0^{(k)} \right)^{-\alpha_r}$ is the path loss of the STAR-RIS aided link. The C_r is the intercept. The α_r is the path loss exponent. $r_i^{(k)}$ denotes the distance between the BS and the assisted STAR-RIS. $d_0^{(k)}$ represents the distance between the STAR-RIS and the UE.

B. UE Association and Channel Power Gain Characterization

We assume that direct communication links of the typical UE u_t are blocked and one STAR-RIS is employed to assist the signal transmission. Specifically, the typical UE associates to the nearest STAR-RIS and the STAR-RIS chooses the strongest BS as the serving BS. The probability density function (PDF) of the serving distance can be given by

$$f_{RU}(x) = 2\pi\lambda_R x \exp(-\pi\lambda_R x^2), \quad (3)$$

$$f_{BR}(x) = 2\pi\lambda_B x \exp(-\pi\lambda_B x^2). \quad (4)$$

Let h_r denote the equivalent overall small-scale fading for the STAR-RIS aided composite channel, whose power is given by

$$|h_r|^2 \triangleq \left| (\mathbf{H}_{RU})^H \tilde{\Theta}^\chi \mathbf{H}_{BR} \right|^2 = \left(\sum_{n=1}^N h_{BR,n} h_{RU,n} \right)^2, \quad (5)$$

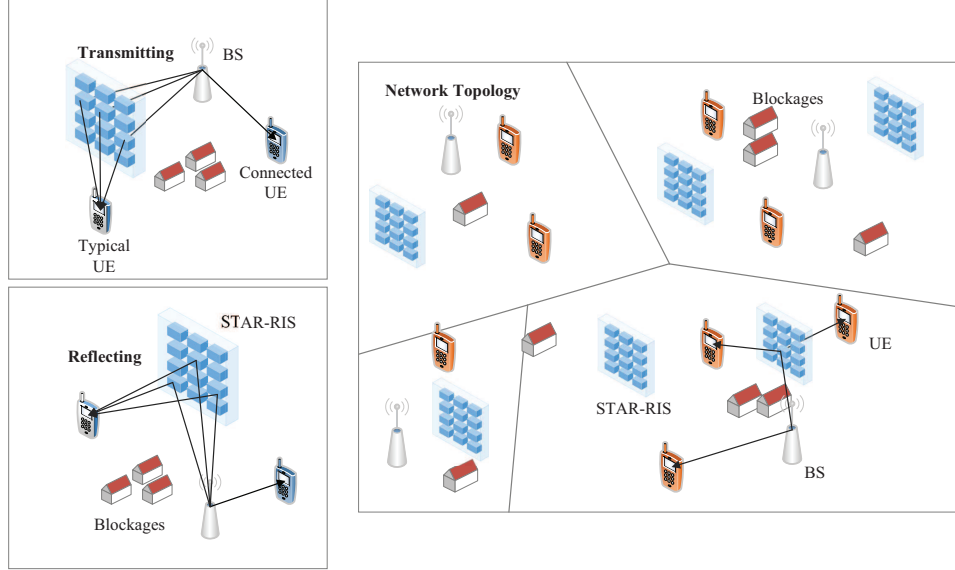


Fig. 1. Illustration of the considered STAR-RIS aided networks: the left two subfigures show the assistant STAR-RIS transmitting and reflecting signals, respectively; the right subfigure depicts the network topology of the STAR-RIS aided networks.

where $\tilde{\Theta}^\chi = \Theta^\chi / \beta^\chi = \text{diag}(e^{j\theta_1^\chi}, e^{j\theta_2^\chi}, \dots, e^{j\theta_N^\chi})$ is the normalized phase-shifting matrix of the STAR-RIS. To maximize the received power, the STAR-RIS adjust the phase shift on each element so that signals from all channels are of the same phase at the typical UE. Thus, the overall CPG for the typical UE can be expressed as $|H_{t,i}^{(k)}|^2 = \beta^\chi L_{t,i}^{(k)} |h_r|^2$.

We assume that the connected UE u_c associates to BS i through the direct communication link and the fixed serving distance is d_c . The overall CPG for the connected UE is hence given by $|H_{c,i}|^2 = L_{c,i} |h_d|^2$.

C. SINR Analysis

We assume that the SIC in a NOMA group is always processed at the typical UE. Let a_t and a_c denote the power allocation coefficients for the typical UE and the connected UE, respectively. Thus, we have $a_t < a_c$ and $a_t + a_c = 1$.

The typical UE first decodes the information of the connected UE in the typical NOMA group with the following SINR

$$\gamma_{t \rightarrow c} = \frac{a_c P_B \beta^\chi L_{t,i}^{(k)} |h_r|^2}{a_t P_B \beta^\chi L_{t,i}^{(k)} |h_r|^2 + I_r + n_0^2}, \quad (6)$$

with

$$I_s = \sum_{m \in \Phi_B^T \setminus i} P_B \beta^T L_{t,m}^{(k)} |h_r|^2 + \sum_{m \in \Phi_B^R \setminus i} P_B \beta^R L_{t,m}^{(k)} |h_r|^2, \quad (7)$$

where n_0^2 is the additive white Gaussian noise (AWGN) power and I_r is the interference from the serving STAR-RIS k . The Φ_B^T and Φ_B^R represent the BS sets of transmitting and reflecting, respectively. We assume that only the STAR-RIS k is pointed at the typical UE, so links between the other STAR-RISs and the typical UE are blocked.

After the SIC process, the decoding SINR at the typical UE can be expressed as

$$\gamma_t = \frac{a_t P_B \beta^X L_{t,i}^{(k)} |h_r|^2}{I_r + n_0^2}. \quad (8)$$

For the connected UE, the signal can be decoded by treating the message transmitted to the typical UE as interference. Therefore, the decoding SINR at the connected UE is as follows

$$\gamma_c = \frac{a_c P_B L_{c,i} |h_d|^2}{a_t P_B L_{c,i} |h_d|^2 + I_d + n_0^2}, \quad (9)$$

with

$$I_d = \sum_{m \in \Phi_B \setminus i} P_B L_{c,m} |h_d|^2, \quad (10)$$

where I_d is the interference for the connected UE.

We focus on the performance of both the typical UE and the connected UE in this work.

III. FITTING THE COMPOSITE SMALL-SCALE FADING POWER

For the STAR-RIS aided link, multiple elements of STAR-RISs introduce the composite channel, the accurate power of which can be intractable for performance analysis in large-scale deployment multi-cell scenarios. In this section, we first provide a tractable fitting method to characterize the distribution of the composite CPG for a general fading case. Some typical cases are then investigated and the fitting results are validated at last.

A. General Small-Scale Fading Model

We begin by considering a general expression of $h_{r,n} = h_{BR,n} h_{RU,n}$. We use μ_r and σ_r^2 to denote the mean and variance of $h_{r,n}$, respectively. Then we can provide the approximated distribution of the composite small-scale fading CPG in the following lemma.

Lemma 1. *The distribution of the overall small-scale fading CPG of the STAR-RIS aided link can be approximated by a Gamma distribution*

$$|h_r|^2 \sim \Gamma \left(\frac{M_r^2}{V_r}, \frac{V_r}{M_r} \right), \quad (11)$$

where $M_r = \mu_r^2 N^2 + \sigma_r^2 N$ and $V_r = 4\mu_r^2 \sigma_r^2 N^3 + 2\sigma_r^4 N^2$.

Proof: Noticed that the small-scale fading for N different channels are independently and identically distributed, the CLT can be employed. Therefore, the distribution of the composite channel gain obeys Gaussian distribution

$$h_r \sim \mathcal{N} (N\mu_r, N\sigma_r^2). \quad (12)$$

For simplicity, we denote $\mu_N = N\mu_r$ and $\sigma_N^2 = N\sigma_r^2$. Thus, the power of this equivalent small-scale fading $|h_r|^2$ obeys noncentral chi-square distribution with the mean $\mathbb{E}[|h_r|^2] = \mu_N^2 + \sigma_N^2$. Considering the fourth order moment of h_r is $\mathbb{E}[|h_r|^4] = \mu_N^4 + 6\mu_N^2\sigma_N^2 + 3\sigma_N^4$, the variance can be calculated by $\text{var}[|h_r|^2] = \mathbb{E}[|h_r|^4] - (\mathbb{E}[|h_r|^2])^2$. Using the method of moments, the distribution of $|h_r|^2$ can be approximated by a Gamma distribution $\Gamma(k_r, \theta_r)$ with the shape parameter and the scale parameter expressed as follows

$$k_r = (\mathbb{E}[|h_r|^2])^2 / \text{var}[|h_r|^2], \quad (13)$$

$$\theta_r = \text{var}[|h_r|^2] / \mathbb{E}[|h_r|^2]. \quad (14)$$

After some algebraic manipulations, this lemma is proved. ■

When the number of STAR-RIS elements is large, we can obtain the following corollary.

Corollary 1. *When N is sufficiently large, the Gamma distribution can be rewritten as*

$$|h_r|^2 \sim \Gamma \left(\frac{\mu_r^2}{4\sigma_r^2} N, 4\sigma_r^2 N \right). \quad (15)$$

Proof: According to Lemma 1, we can calculate that $\frac{M_r^2}{V_r} = \frac{\mu_r^2}{4\sigma_r^2} N + o(1)$ and $\frac{V_r}{M_r} = 4\sigma_r^2 N + o(1)$. Then (15) is obtained. ■

Remark 1. *It can be found from Corollary 1 that both the shape and scale parameter are in proportion to the number of STAR-RIS elements. Furthermore, let us recall the property of the*

Gamma distribution, by which $\Gamma\left(\frac{\mu_r^2}{4\sigma_r^2}N, 4\sigma_r^2N\right) = \mu_r^2N^2\Gamma\left(\frac{\mu_r^2N}{4\sigma_r^2}, \frac{4\sigma_r^2}{\mu_r^2N}\right)$. As $N \rightarrow \infty$, we have

$$\frac{|h_r|^2}{\mathbb{E}[|h_r|^2]} \sim \Gamma\left(\frac{\mu_r^2N}{4\sigma_r^2}, \frac{4\sigma_r^2}{\mu_r^2N}\right) \rightarrow 1, \quad (16)$$

which shows the channel hardening effect of the STAR-RIS aided link. Therefore, with the increase of N , the CPG asymptotically approaches a deterministic value.

B. Case Studies

In this subsection, we pay our attention to some typical small-scale fading models. When the parameters of the particular distribution are predefined, we can easily derive the fitted Gamma distribution. For the cases N is large, simple asymptotic expressions can be obtained based on Corollary 1. The results are concluded in table I. Detailed discussions between channel parameters and analytical fitting results are as follows.

1) *Rayleigh Channel*: The channel gain of the Rayleigh channel obeys the Rayleigh distribution with the scale parameter $\delta_1 > 0$. We can find that the shape parameter k_r of the fitted Gamma distribution is unrelated to Rayleigh parameter δ_1 .

2) *Nakagami- m Channel*: In this case, the channel gain obeys the Nakagami distribution with the shape parameter $m_2 \geq \frac{1}{2}$ and the scale parameter $\Omega_2 > 0$. The result shows that k_r is related to m_2 but not related to Ω_2 .

3) *Rician Channel*: According to [8], the channel gain of the Rician channel shown as follows consists of two portions

$$h_{r,n} = \sqrt{\frac{K_3}{K_3 + 1}}h_{r,n}^{\text{LoS}} + \sqrt{\frac{1}{K_3 + 1}}h_{r,n}^{\text{NLoS}}, \quad (17)$$

where K_3 is the Rician fading factor. $h_{r,n}^{\text{LoS}} = c_3$ is the deterministic LoS component. $h_{r,n}^{\text{NLoS}}$ is the random NLoS component modeled as Rayleigh fading with the scale parameter $\delta_3 > 0$. Therefore, the Rician channel considers impacts of both LoS transmissions and NLoS transmissions.

4) *Weibull Channel*: For the Weibull channel, the channel gain obeys the Weibull distribution with the shape parameter $k_4 > 0$ and the scale parameter $\lambda_4 > 0$. It can be found that k_r is only related to the shape parameter k_4 .

TABLE I
TYPICAL SMALL-SCALE FADING MODELS

| Models | Channel Parameters | μ_r | σ_r^2 | Gamma Distributions (N is large) |
|-------------------------|--------------------------------------|---------------------------------------------------------------------------------------------------|-----------------------------------------------------------------------------------------|------------------------------------------------------------------------------------------------------------------------------------------------------------------------------------------------------------------------|
| Rayleigh Channel | $\delta_1 > 0$ | $\delta_1 \sqrt{\frac{\pi}{2}}$ | $\frac{4-\pi}{2} \delta_1^2$ | $k_r = \frac{\pi}{4(4-\pi)} N, \theta_r = 2(4-\pi)\delta_1^2 N$ |
| Nakagami- m Channel | $m_2 \geq \frac{1}{2}, \Omega_2 > 0$ | $\frac{\Gamma(m_2 + \frac{1}{2})}{\Gamma(m_2)} \left(\frac{\Omega_2}{m_2} \right)^{\frac{1}{2}}$ | $\frac{\Omega_2 -}{m_2} \left(\frac{\Gamma(m_2 + \frac{1}{2})}{\Gamma(m_2)} \right)^2$ | $k_r = \frac{\Gamma(m_2 + \frac{1}{2})^2}{4(m_2 \Gamma(m_2)^2 - \Gamma(m_2 + \frac{1}{2})^2)} N,$ $\theta_r = 4\Omega_2 N - \frac{4\Omega_2}{m_2} \left(\frac{\Gamma(m_2 + \frac{1}{2})}{\Gamma(m_2)} \right)^2 N$ |
| Rician Channel | $K_3 > 0, \delta_3 > 0, c_3 > 0$ | $\delta_3 \sqrt{\frac{\pi}{2}} \sqrt{\frac{1}{K_3+1}} + c_3 \sqrt{\frac{K_3}{K_3+1}}$ | $\frac{4-\pi}{2} \frac{\delta_3^2}{K_3+1}$ | $k_r = \frac{\pi \delta_3^2 + 4\delta_3 c_3 \sqrt{\frac{\pi}{2} K_3} + 2K_3 c_3^2}{4(4-\pi) \delta_3^2} N,$ $\theta_r = \frac{2(4-\pi) \delta_3^2}{K_3+1} N$ |
| Weibull Channel | $k_4 > 0, \lambda_4 > 0$ | $\lambda_4 \Gamma(1 + \frac{1}{k_4})$ | $\lambda_4^2 \left(\Gamma(1 + \frac{2}{k_4}) - \Gamma(1 + \frac{1}{k_4})^2 \right)$ | $k_r = \frac{\Gamma(1 + \frac{1}{k_4})^2}{\Gamma(1 + \frac{2}{k_4}) - \Gamma(1 + \frac{1}{k_4})^2} \frac{N}{4}, \theta_r = 4\lambda_4^2 \left(\Gamma(1 + \frac{2}{k_4}) - \Gamma(1 + \frac{1}{k_4})^2 \right) N$ |
| Double-Rayleigh Channel | $\delta_5 > 0, \delta_6 > 0$ | $\frac{\pi \delta_5 \delta_6}{2}$ | $4(1 - \frac{\pi^2}{16}) \delta_5^2 \delta_6^2$ | $k_r = \frac{\pi^2}{64(1 - \pi^2/16)} N,$ $\theta_r = (16 - \pi^2) \delta_5^2 \delta_6^2 N$ |

5) *Double-Rayleigh Channel*: In RIS-enabled communications, the cascaded channel is introduced. In fact, the small-scale fading correlates to channel conditions of two parts of the cascaded RIS aided link, although small-scale fading models have been simplified in some works. Let us consider the double-Rayleigh channel as a example, which is the product of two independent Rayleigh channels. Similar to the result of Rayleigh channel, k_r is unrelated to any Rayleigh parameter δ_5 or δ_6 .

C. Fitting Accuracy

To validate the accuracy of the proposed fitting method, we plot the cumulative distribution function (CDF) of $|h_r|^2$ in Fig. 2. Five different small-scale fading models as we discussed in section III-B are considered. In Fig. 2, we use lines to present the Monte Carlo simulation results and marks to depict the analytical fitting results. The simulation parameters are set as: $\delta_1 = \delta_3 = \delta_5 = \delta_6 = \sqrt{\frac{1}{2}}, m_2 = k_4 = 4, \Omega_2 = K_3 = c_3 = \lambda_4 = 1$.

We can observe that the fitted Gamma distributions shown in Lemma 1 and Corollary 1 become more accurate with a larger number of STAR-RIS elements. This can be attributable to the application of CLT. For both cases $N = 9$ and $N = 64$, the analytical results provided in

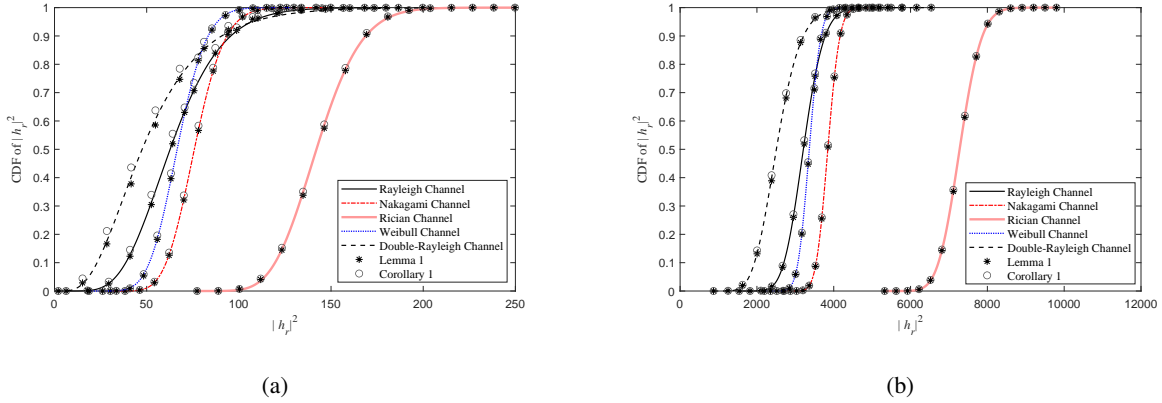


Fig. 2. CDF versus the value of $|h_r|^2$ with different small-scale fading models: (a) the number of STAR-RIS elements $N = 9$; (b) the number of STAR-RIS elements $N = 64$.

Lemma 1 fits the numerical results well, while the results in Corollary 1 should be applied in large N cases.

IV. COVERAGE PROBABILITY

In this section, we derive the general expressions of the coverage probability for the typical UE and the connected UE. For comparison, the results in traditional RIS aided networks are also obtained.

Based on the previous analysis in Section III, the composite small-scale fading power of the STAR-RIS aided link can be fitted by Gamma distribution $\Gamma(k_r, \theta_r)$. Different from the power distribution of the Nakagami- m fading channel in traditional networks, $\Gamma(k_r, \theta_r)$ is a general Gamma distribution and the value of k_r might be very large. Therefore, Alzer's inequality [36] employed in most existing works is no longer efficient in our scenarios. Although the Gil-Pelaez theorem is available for arbitrary distributions [37], an extra fold of integral is introduced, which brings challenges to obtain insights from the complex analytical expressions. Sparked by above reasons, we provide a novel analytical method in this work.

Before deriving the performance expressions, let us introduce some preliminary definitions.

Definition 1. For a non-negative integer m , we use $\xi_m(a, b, c; x)$ to describe the following

expression related to the Gauss hypergeometric function

$$\xi_m(a, b, c; x) \triangleq \frac{(a)_m(-2/b)_m(-c)^m}{(1-2/b)_m} {}_2F_1\left(a, -\frac{2}{b}; 1-\frac{2}{b}; -cx\right), \quad (18)$$

where $(x)_m$ is the Pochhammer's symbol. If $m = 0$, $(x)_0 = 1$; otherwise, $(x)_m = x(x+1)\cdots(x+m-1)$.

Definition 2. We define \bar{k}_s as the nearest positive integer of k_r , which satisfies

$$\bar{k}_s = \arg \min_x |x - k_r|, x \in \mathbb{N}^+. \quad (19)$$

A. Laplace Transform of Interference

Since the Laplace transform of the interference is the essential part of the coverage probability, we derive these expressions first.

The typical UE suffers the interference I_r that consists of two portions: 1) transmissive interference from the BSs located at the back of the serving STAR-RIS; and 2) reflective interference from the BSs which are in front of the serving STAR-RIS. This Laplace transform is presented in the following lemma.

Lemma 2. In STAR-RIS aided networks, the Laplace transform of the interference for the typical UE can be derived as

$$\begin{aligned} \mathcal{L}_{I_r}(s) &= \exp\left(-\frac{1}{2}\pi\lambda_B r_t^2 (\xi_0(k_r, \alpha_r, \beta^T \eta_t; s) - 1)\right) \\ &\quad \times \exp\left(-\frac{1}{2}\pi\lambda_B r_t^2 (\xi_0(k_r, \alpha_r, \beta^R \eta_t; s) - 1)\right), \end{aligned} \quad (20)$$

where $\eta_t = \theta_r P_B L_{0,i}^{(k)}$.

Proof: See Appendix A. ■

If the RIS is reflecting-only, the typical UE suffers the interference I_r^{ref} from half of the space.

Lemma 3. In traditional RIS aided networks, the Laplace transform of the interference for the typical UE can be derived as

$$\mathcal{L}_{I_r^{ref}}(s) = \exp\left(-\frac{1}{2}\pi\lambda_B r_t^2 (\xi_0(k_r, \alpha_r, \eta_t; s) - 1)\right). \quad (21)$$

Proof: The proof is similar to Lemma 2. ■

For the connected UE, the interference I_d is from the direct links between the connected UE and the interfering BSs with Rayleigh fading channels. In the following proposition, we provide the Laplace transform of I_d .

Proposition 1. *The Laplace transform of the interference for the connected UE can be given by*

$$\mathcal{L}_{I_d}(s) = \exp\left(-\pi\lambda_B d_c^2 (\xi_0(1, \alpha_d, \eta_c; s) - 1)\right), \quad (22)$$

where $\eta_c = P_B L_{c,i}$.

B. Coverage Performance for the Typical UE

In this work, the coverage probability for the typical UE is defined as the probability that the typical UE can successfully transmit signals with a targeted SINR τ_t . The typical UE only decodes its own message after a successful SIC process. The coverage probability can be expressed as

$$P_{cov,t} = \mathbb{P}(\gamma_{t \rightarrow c} > \tau_c, \gamma_t > \tau_t), \quad (23)$$

where τ_c is the target SINR for the connected UE.

Considering the signal transmission mode at the serving STAR-RIS for the typical UE is $\chi \in \{T, R\}$, the conditional coverage probability of the typical UE can be rewritten as

$$P_{cov,t}^{\chi} \Big|_{d_{0,i}^{(k)}} = \mathbb{P}\left(|h_r|^2 > \tau_t^* \frac{I_r + n_0^2}{\beta^{\chi} P_B L_{0,i}^{(k)}}\right), \quad (24)$$

where $\tau_t^* = \max\left(\frac{\tau_c}{a_c - \tau_{cat}}, \frac{\tau_t}{a_t}\right)$.

Utilizing the scaling feature of the Gamma distribution, we have $\frac{1}{\theta_r} |h_r|^2 \sim \Gamma(k_r, 1)$. However, k_r is not an integer in most cases. For tractability, we introduce \bar{k}_r defined in Definition 2 to deduce the analytical coverage expressions.

Theorem 1. *In STAR-RIS aided networks, the coverage probability for the typical UE is derived as*

$$\begin{aligned} P_{cov,t} &= \int_0^{\infty} \int_0^{\infty} \pi \lambda_B r_1 f_{RU}(r_2) \sum_{m=0}^{\bar{k}_r-1} \frac{(-1)^m}{m!} \exp\left(V_T^{(0)}(1)\right) \mathcal{B}_m \left(V_T^{(1)}(1), \dots, V_T^{(m)}(1)\right) dr_1 dr_2 \\ &+ \int_0^{\infty} \int_0^{\infty} \pi \lambda_B r_1 f_{RU}(r_2) \sum_{m=0}^{\bar{k}_r-1} \frac{(-1)^m}{m!} \exp\left(V_R^{(0)}(1)\right) \mathcal{B}_m \left(V_R^{(1)}(1), \dots, V_R^{(m)}(1)\right) dr_1 dr_2, \end{aligned} \quad (25)$$

with

$$V_{\chi}^{(m)}(x) = -\Delta^{(m)} - \frac{1}{2}\pi r_1^2 \lambda_B \xi_m(k_r, \alpha_r, D_{\chi}^T; x) - \frac{1}{2}\pi r_1^2 \lambda_B \xi_m(k_r, \alpha_r, D_{\chi}^R; x), \quad (26)$$

where $\mathcal{B}_m(x_1, \dots, x_m)$ is the m th complete Bell polynomial. $D_{\chi}^T = \frac{\tau_t^* \beta^T}{\beta^{\chi}}$, $D_{\chi}^R = \frac{\tau_t^* \beta^R}{\beta^{\chi}}$, and $s_{\chi} = \frac{\tau_t^* (r_1 r_2)^{\alpha_r}}{\theta_r \beta^{\chi} P_B C_r}$. $\Delta^{(0)} = s_{\chi} n_0^2 x$, $\Delta^{(1)} = s_{\chi} n_0^2$, and $\Delta^{(m)} = 0$ when $m \geq 2$.

Proof: See Appendix B. ■

In STAR-RIS aided communications, the operating parameters make difference to the system performance. Thus, the following corollary provides the optimal energy splitting coefficient in terms of coverage performance.

Corollary 2. *When $\beta^T = \beta^R = \frac{1}{2}$, the maximum coverage probability of the typical UE is*

$$P_{cov,t}^{\max} = \int_0^{\infty} \int_0^{\infty} 2\pi \lambda_B r_1 f_{RU}(r_2) \sum_{m=0}^{\bar{k}_r-1} \frac{(-1)^m}{m!} \exp\left(\tilde{V}^{(0)}(1)\right) \mathcal{B}_m\left(\tilde{V}^{(1)}(1), \dots, \tilde{V}^{(m)}(1)\right) dr_1 dr_2, \quad (27)$$

where $\tilde{V}^{(m)}(x) = -\Delta^{(m)} - \pi r_1^2 \lambda_B \xi_m(k_r, \alpha_r, \tau_t^*; x)$.

Proof: See Appendix C. ■

Remark 2. *The results obtained in Corollary 2 can be explained that when $\beta^T = \beta^R = \frac{1}{2}$, the typical UE can always associate to the BS with the maximum average received power $\beta^{\chi} P_B L_{t,i}^{(k)}$. This illustrates that the system coverage can be optimized by adjusting the energy splitting coefficient of STAR-RISs. Furthermore, based on the capability of controlling the signal power, STAR-RISs can meet various QoS requirements of different UEs.*

Theorem 2. *In traditional RIS aided networks, the coverage probability for the typical UE is derived as*

$$P_{cov,t}^{ref} = \int_0^{\infty} \int_0^{\infty} \pi \lambda_B r_1 f_{RU}(r_2) \sum_{m=0}^{\bar{k}_r-1} \frac{(-1)^m}{m!} \exp\left(V_{ref}^{(0)}(1)\right) \mathcal{B}_m\left(V_{ref}^{(1)}(1), \dots, V_{ref}^{(m)}(1)\right) dr_1 dr_2, \quad (28)$$

with

$$V_{ref}^{(m)}(x) = -\Delta_{ref}^{(m)} - \frac{1}{2}\pi r_1^2 \lambda_B \xi_m(k_r, \alpha_r, \tau_t^*; x), \quad (29)$$

where $s_{ref} = \frac{\tau_t^*(r_1 r_2)^{\alpha_r}}{\theta_r P_B C_r}$, $\Delta_{ref}^{(0)} = s_{ref} n_0^2 x$, $\Delta_{ref}^{(1)} = s_{ref} n_0^2$, and $\Delta_{ref}^{(m)} = 0$ when $m \geq 2$.

Proof: Since the assisted reflecting-only RIS must locate at the same half-space of the typical UE, the PDF of the serving distance between the BS and the assistant RIS is

$$f_{BR}^{ref}(x) = \pi \lambda_b x \exp\left(-\frac{1}{2} \lambda_b x^2\right). \quad (30)$$

Then, using the similar proof in Theorem 1 and (21), this theorem can be proved. \blacksquare

Now let us consider the interference-limited case as a special case. In this case, the noise is negligible compared to the interference, i.e. $I_r \gg n_0^2$, so we focus on SIR coverage. We can obtain closed-form expressions for the coverage probability of the typical UE shown as the following corollaries.

Corollary 3. *When $I_r \gg n_0^2$, the coverage probability of the typical UE in STAR-RIS aided networks can be expressed in a closed form as follows*

$$\begin{aligned} P_{cov,t} = & \sum_{m=0}^{\bar{k}_r-1} \frac{(-1)^m}{m!} \sum_{l=1}^m \frac{(-1)^l l!}{\left(V_{SIR,T}^{(0)}(1)\right)^{l+1}} \mathcal{B}_{m,l} \left(V_{SIR,T}^{(1)}(1), \dots, V_{SIR,T}^{(m-l+1)}(1)\right) \\ & + \sum_{m=0}^{\bar{k}_r-1} \frac{(-1)^m}{m!} \sum_{l=1}^m \frac{(-1)^l l!}{\left(V_{SIR,R}^{(0)}(1)\right)^{l+1}} \mathcal{B}_{m,l} \left(V_{SIR,R}^{(1)}(1), \dots, V_{SIR,R}^{(m-l+1)}(1)\right), \end{aligned} \quad (31)$$

where $V_{SIR,\chi}^{(m)}(x) = \xi_m(k_r, \alpha_r, D_\chi^T; x) + \xi_m(k_r, \alpha_r, D_\chi^R; x)$.

Proof: Since the operators of integral and differentiation are interchangeable, we can calculate the second-order derivative of the conditional coverage probability for $\chi \in \{T, R\}$

$$P_{cov,t}^\chi = \sum_{m=0}^{\bar{k}_r-1} \frac{(-1)^m}{m!} \left[\frac{\partial^m}{\partial x^m} \frac{2}{\xi_0(k_r, \alpha_r, D_\chi^T; x) + \xi_0(k_r, \alpha_r, D_\chi^R; x)} \right]_{x=1}. \quad (32)$$

Then we recall Faà di Bruno's formula as we have stated in the proof of Theorem 1, this corollary is proved. \blacksquare

Remark 3. *It can be observed from (31) that the coverage probability is unrelated to the scale parameter θ_r in the interference limited scenario. In this case, we only need to calculate the shape parameter k_r when evaluating the Gamma distribution of the composite small-scale fading power. The value of k_r for some typical small-scale fading models has been discussed in Section III-B.*

Corollary 4. When $I_r \gg n_0^2$, the coverage probability of the typical UE in traditional RIS aided networks can be expressed in a closed form as follows

$$P_{cov,t}^{ref} = \sum_{m=0}^{k_r-1} \frac{(-1)^m}{m!} \sum_{l=1}^m \frac{(-1)^l l!}{\left(V_{SIR,ref}^{(0)}(1)\right)^{l+1}} \mathcal{B}_{m,l} \left(V_{SIR,ref}^{(1)}(1), \dots, V_{SIR,ref}^{(m-l+1)}(1) \right), \quad (33)$$

where $V_{SIR,ref}^{(m)}(x) = \xi_m(k_r, \alpha_r, \tau_t^*; x)$.

Proof: The proof is similar to Corollary 3. ■

Remark 4. By observing (31) and (33) we can find that when $\beta^T = \beta^R = \frac{1}{2}$, the value of coverage probability in two kinds of RIS aided networks are equal. Therefore, (33) is the tight upper bound for (31) in interference-limited scenarios.

C. Coverage Performance for the Connected UE

The connected UE decodes its own message by treating the typical UE as noise, so the coverage probability is

$$P_{cov,c} = \mathbb{P}(\gamma_c > \tau_c). \quad (34)$$

Based on (9), the coverage probability of the connected UE can be rewritten as

$$P_{cov,c}|_{d_c} = \mathbb{P} \left(|h_d|^2 > \tau_c^* \frac{I_r + n_0^2}{P_B L_{c,i}} \right), \quad (35)$$

where $\tau_c^* = \frac{\tau_c}{a_c - a_t \tau_c}$.

Since the connected UE experiences the Rayleigh fading without the assistance of the STAR-RIS, we can easily obtain the exact analytical expression shown in the following proposition.

Proposition 2. The coverage probability for the connected UE can be given by

$$P_{cov,c} = \exp \left(-\pi \lambda_B d_c^2 (\xi_0(1, \alpha_d, \tau_c^*; 1) - 1) \right) \exp \left(-\frac{\tau_c^* n_0^2}{P_B C_d d_c^{-\alpha_d}} \right). \quad (36)$$

V. ERGODIC RATE

Rather than calculating the coverage probability with a predefined threshold, the ergodic rate of the STAR-RIS aided NOMA networks is determined by random channel conditions of UEs. Hence the ergodic rate can be an important metric to characterize the system performance. In this section, we evaluate the ergodic rates for both the typical UE and the connected UE. Besides, the results in traditional RIS aided networks are also obtained.

A. Ergodic Rate for the Typical UE

According to our assumption, the SIC procedure always occurs at the typical UE. If the typical UE fails to processes the SIC, it can never decode its own message hence its ergodic rate is zero. Therefore, the ergodic rate of the typical UE can be expressed as

$$R_t = \mathbb{E} [\log_2 (1 + \gamma_t), \gamma_{t \rightarrow c} > \tau_c]. \quad (37)$$

Based on the expressions of the coverage probability, we can obtain the exact ergodic rate in two kinds of RIS aided networks in Theorem 3 and Theorem 4.

Theorem 3. *In STAR-RIS aided networks, the ergodic rate for the typical UE is derived as*

$$R_t = \frac{1}{\ln 2} \int_{a_t \tau_c^*}^{\infty} \frac{\bar{F}_t(z)}{1+z} dz + \log_2 (1 + a_t \tau_c^*) \bar{F}_t(a_t \tau_c^*), \quad (38)$$

where $\bar{F}_t(z)$ is given by

$$\begin{aligned} \bar{F}_t(z) = & \int_0^{\infty} \int_0^{\infty} \pi \lambda_B r_1 f_{RU}(r_2) \sum_{m=0}^{\bar{k}_r-1} \frac{(-1)^m}{m!} \exp \left(\Lambda_T^{(0)}(z) \right) \mathcal{B}_m \left(\Lambda_T^{(1)}(z), \dots, \Lambda_T^{(m)}(z) \right) dr_1 dr_2 \\ & + \int_0^{\infty} \int_0^{\infty} \pi \lambda_B r_1 f_{RU}(r_2) \sum_{m=0}^{\bar{k}_r-1} \frac{(-1)^m}{m!} \exp \left(\Lambda_R^{(0)}(z) \right) \mathcal{B}_m \left(\Lambda_R^{(1)}(z), \dots, \Lambda_R^{(m)}(z) \right) dr_1 dr_2, \end{aligned} \quad (39)$$

here the $\Lambda_{\chi}^{(m)}(z)$ is

$$\Lambda_{\chi}^{(m)}(z) = -\Delta_{rate}^{(m)} - \frac{1}{2} \pi r_1^2 \lambda_B \xi_m \left(k_r, \alpha_r, \frac{\beta^T z}{a_t \beta^{\chi}}; 1 \right) - \frac{1}{2} \pi r_1^2 \lambda_B \xi_m \left(k_r, \alpha_r, \frac{\beta^R z}{a_t \beta^{\chi}}; 1 \right). \quad (40)$$

Besides, $\Delta_{rate}^{(m)} = \frac{(r_1 r_2)^{\alpha_r} z}{a_t \theta_r \beta^{\chi} P_B C_r}$ when $m < 2$, and $\Delta_{rate}^{(m)} = 0$ when $m \geq 2$.

Proof: See Appendix D. ■

We also investigate the impact of the energy splitting coefficient on the ergodic rate in the following corollary.

Corollary 5. *When $\beta^T = \beta^R = \frac{1}{2}$, the maximum ergodic rate of the typical UE is*

$$R_t^{\max} = \frac{1}{\ln 2} \int_{a_t \tau_c^*}^{\infty} \frac{\bar{F}_t^{\max}(z)}{1+z} dz + \log_2 (1 + a_t \tau_c^*) \bar{F}_t^{\max}(a_t \tau_c^*), \quad (41)$$

where $\bar{F}_t^{\max}(z)$ is expressed as

$$\begin{aligned} \bar{F}_t^{\max}(z) = & \int_0^{\infty} \int_0^{\infty} 2 \pi \lambda_B r_1 f_{RU}(r_2) \\ & \times \sum_{m=0}^{\bar{k}_r-1} \frac{(-1)^m}{m!} \exp \left(\tilde{\Lambda}^{(0)}(z) \right) \mathcal{B}_m \left(\tilde{\Lambda}^{(1)}(z), \dots, \tilde{\Lambda}^{(m)}(z) \right) dr_1 dr_2, \end{aligned} \quad (42)$$

and $\tilde{\Lambda}^{(m)}(z) = -\Delta_{rate}^{(m)} - \pi r_1^2 \lambda_B \xi_m \left(k_r, \alpha_r, \frac{z}{a_t}; 1 \right)$.

Proof: We denote $\beta = \beta^T = 1 - \beta^R$. Following the similar procedure of the proof in Corollary 2, we can calculate $\frac{\partial}{\partial \beta} R_t^{\max}$ and find that $\frac{\partial}{\partial \beta} R_t^{\max} = 0$ when $\beta = \frac{1}{2}$. Then the maximum ergodic rate is obtained. \blacksquare

Remark 5. Similar to the results in coverage probability, when $\beta^T = \beta^R = \frac{1}{2}$, the typical UE associates to the BS with maximum average received power, and the ergodic rate can be maximized. Thus, the appropriate energy splitting coefficient of STAR-RISs helps to improve the achievable ergodic rate.

Theorem 4. In traditional RIS aided networks, the ergodic rate for the typical UE is derived as

$$R_t^{ref} = \frac{1}{\ln 2} \int_{a_t \tau_c^*}^{\infty} \frac{\bar{F}_t^{ref}(z)}{1+z} dz + \log_2(1 + a_t \tau_c^*) \bar{F}_t^{ref}(a_t \tau_c^*), \quad (43)$$

where $\bar{F}_t^{ref}(z)$ is expressed as

$$\bar{F}_t^{ref}(z) = \int_0^{\infty} \int_0^{\infty} \pi \lambda_B r_1 f_{RU}(r_2) \sum_{m=0}^{\bar{k}_r-1} \frac{(-1)^m}{m!} \exp\left(\Lambda_{ref}^{(0)}(z)\right) \mathcal{B}_m \left(\Lambda_{ref}^{(1)}(z), \dots, \Lambda_{ref}^{(m)}(z) \right) dr_1 dr_2, \quad (44)$$

the $\Lambda_{ref}^{(m)}(z)$ is

$$\Lambda_{ref}^{(m)}(z) = -\Delta_{rate,ref}^{(m)} - \pi r_1^2 \lambda_B \xi_m \left(k_r, \alpha_r, \frac{z}{a_t}; 1 \right). \quad (45)$$

Besides, $\Delta_{rate,ref}^{(m)} = \frac{(r_1 r_2)^{\alpha_r} z}{a_t \theta_r P_B C_r}$ when $m < 2$, and $\Delta_{rate,ref}^{(m)} = 0$ when $m \geq 2$.

Proof: The proof is similar to Theorem 3. \blacksquare

Remark 6. Note that $\bar{F}_t(z) = P_{cov,t}(\frac{z}{a_t})$ and $\bar{F}_t^{ref}(z) = P_{cov,t}^{ref}(\frac{z}{a_t})$, the expressions of the ergodic rate come from the coverage probability. Therefore, we can obtain the similar conclusion as in coverage probability. Based on (31), (33), and Corollary 5, we can find that when $I_r \gg n_0^2$, the ergodic rate in traditional RIS aided networks is the tight upper bound of that in STAR-RIS aided scenarios.

B. Ergodic Rate for the Connected UE

For the connected UE, the ergodic rate can be expressed as

$$R_c = \mathbb{E} [\log_2 (1 + \gamma_c)]. \quad (46)$$

The exact expression of the ergodic rate can be derived based on the coverage probability (36) as follows.

Corollary 6. *The ergodic rate for the connected UE is derived as*

$$R_c = \frac{1}{\ln 2} \int_0^{\frac{a_c}{a_t}} \frac{\bar{F}_c(z)}{1+z} dz, \quad (47)$$

where $\bar{F}_c(z)$ is given by

$$\bar{F}_c(z) = \exp \left(-\pi \lambda_B d_c^2 \left(\xi_0 \left(1, \alpha_d, \frac{z}{a_c - a_t z}; 1 \right) - 1 \right) \right) \exp \left(-\frac{z n_0^2 d_c^{\alpha_d}}{(a_c - a_t z) P_B C_d} \right). \quad (48)$$

Proof: The complementary cumulative distribution function (CCDF) of the decoding SINR for the connected UE is denoted as $\bar{F}_c(z)$, which can be expressed as

$$\bar{F}(z) = \mathbb{P} \left((a_c - a_t z) |h_d|^2 > \frac{(I_r + n_0^2) z}{P_B C_d r^{-\alpha_d}} \right). \quad (49)$$

Note that for the case $z \geq \frac{a_c}{a_t}$, $\bar{F}_c(z) = 0$ always holds. For the case $z < \frac{a_c}{a_t}$, we can obtain (47) by using the similar proof in Theorem 3. \blacksquare

VI. NUMERICAL RESULTS

In this section, we first present the numerical results to verify our analytical expressions derived in previous sections and then provide some interesting insights. For small-scale fading model, we mainly focus on the Rician fading channel as we discussed in Section III. Without otherwise stated, the simulation parameters are defined as follows. The transmit power P_B is 30 dBm. The densities of BSs and STAR-RISs are 50 km^{-2} and 500 km^{-2} , respectively. The path loss exponents are $\alpha_r = 3$ and $\alpha_d = 4$. The intercepts are $C_r = C_d = -30 \text{ dB}$. The target rate is set to be equal as $\rho_t = \rho_c = 0.1$ bit per channel use (BPCU) for the typical UE and the connected UE. Thus, the target SINR are $\tau_t = 2^{\rho_t} - 1$ and $\tau_c = 2^{\rho_c} - 1$. The power allocation coefficients are $a_t = 0.4$ and $a_c = 0.6$. The energy splitting coefficients are $\beta^T = \beta^R = \frac{1}{2}$. The number of STAR-RIS elements is $N = 9$.

A. Validation and Simulations

Validation of analytical expressions of the coverage probability for the typical UE and the connected UE are illustrated in Fig. 3 with different power allocation coefficients. We use lines to present the analytical results and marks to depict the Monte Carlo simulations. We set noise

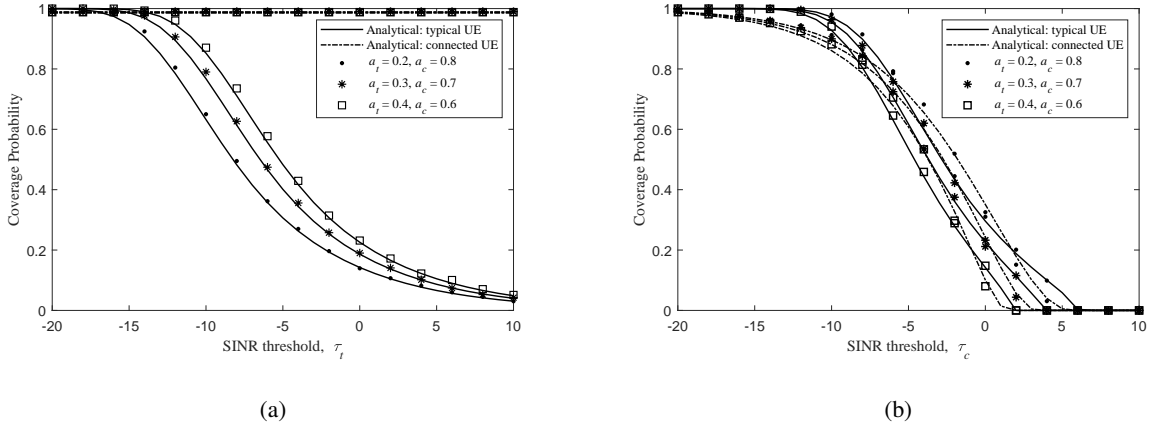


Fig. 3. Coverage probability versus SINR threshold with different power allocation coefficients: (a) the target SINR for the typical UE τ_t ; (b) the target SINR for the connected UE τ_c .

power $n_0^2 = -107$ dBm. In Fig. 3(a) we vary the SINR threshold for the typical UE while in Fig. 3(b) we vary the counterpart for the connected UE. Although the STAR-RIS elements number is not so large, the analytical results fit the simulation curves well.

Due to the limited computing precision of Matlab, it is difficult to calculate the analytical results of the ergodic rate under the predefined parameter setup. However, according to the proof of Theorem 3 we can find that the expression of is from the coverage probability for the typical UE. Therefore, the validation of analytical expressions for the coverage probability guarantees the accuracy of results for the ergodic rate.

B. Impact of Energy Splitting Coefficients

Here, we focus on the impact of energy splitting coefficients under different noise power levels. Fig. 4 and Fig. 5 plot the coverage probability and the ergodic rate for the typical UE versus the energy splitting coefficient for transmitting β^T , respectively; two noise power levels are considered, i.e. $n_0^2 = -80$ dBm and $n_0^2 = -107$ dBm. One can observe that for the STAR-RIS aided scenarios, two kinds of performance are simultaneously maximized when $\beta^T = \frac{1}{2}$, which has been discussed in Corollary 2 and Corollary 5. Besides, the curves are symmetric about $\beta^T = \frac{1}{2}$.

The performance of traditional RIS aided networks is also shown in these figures for comparison. When the noise power is low, the traditional RIS aided networks always outperform

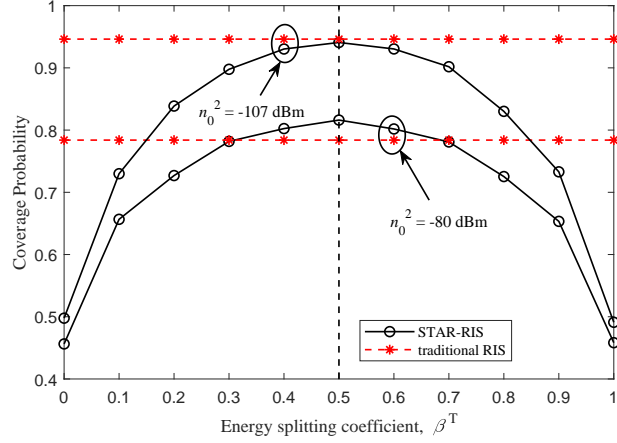


Fig. 4. Coverage probability for the typical UE versus energy splitting coefficient.

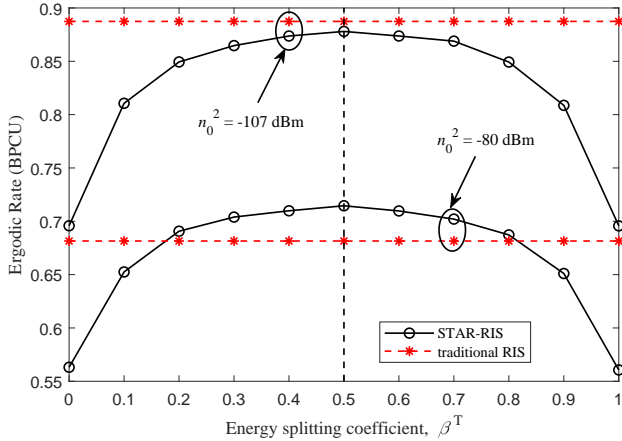


Fig. 5. Ergodic rate for the typical UE versus energy splitting coefficient.

the STAR-RIS aided ones. When the noise power is high, there exists a specific range of β^T to ensure the better performance provided by STAR-RISs. In this case, STAR-RISs brought the performance enhancement as well as the flexibility for communication system designs.

C. Comparison among Different Scenarios

In Fig. 6, we plot coverage probabilities versus transmit SNR in multiple scenarios, where different kinds of RISs and multiple access techniques are considered. For the reference received SNR, we use the average serving distances as the reference distances, i.e., $\bar{d}_t = 22.36$ m, $\bar{r}_t = 70.71$ m. Then we can calculate that the reference path loss is -125 dB. We observe that

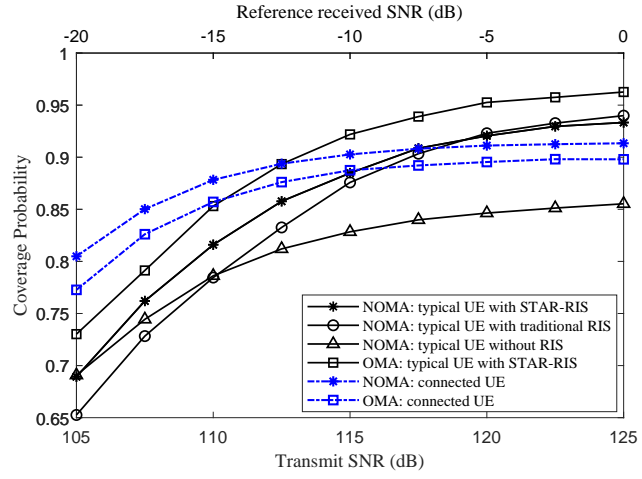


Fig. 6. Coverage probability versus transmit SNR: a comparison among different kinds of RISs and multiple access schemes.

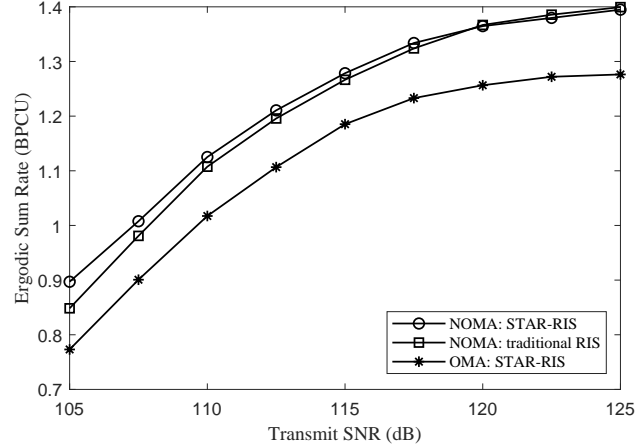


Fig. 7. Ergodic sum rate versus transmit SNR: a comparison among different kinds of RISs and multiple access schemes.

the deployment of RISs improve the coverage for the typical UE, which can be explained that RIS aided links provide superior channel gains. Interestingly, in low SNR cases, STAR-RISs have the better performance than traditional RISs but in high SNR scenarios the conclusion is opposite. Compared with OMA, NOMA enhances the coverage probability of the connected UE. This enhancement comes from the higher power allocated to the connected UE who has the worse channel condition in NOMA systems.

In Fig. 7, we compare ergodic sum rate of the typical UE and the connected UE versus

transmit SNR for STAR-RIS aided NOMA networks, traditional RIS aided NOMA networks, and STAR-RIS aided OMA networks. We can observe that NOMA systems always outperform OMA systems because of their high bandwidth efficiency. Similar to the observation in coverage probability, STAR-RISs achieve higher ergodic sum rate than traditional RISs in low SNR cases.

VII. CONCLUSION

In this paper, a fitting method has been proposed to approximate the distribution of the RIS aided composite CPG. Then, a general analytical framework has been provided to evaluate the coverage probability and the ergodic rate of STAR-RIS aided NOMA multi-cell networks. Theoretical expressions in traditional RIS-aided networks have been obtained for comparison. For more insights, we have investigated the impact of energy splitting coefficients and considered the interference-limited scenario as a special case. The analytical results have revealed that: 1) appropriate energy splitting coefficients can simultaneously improve the system coverage and the ergodic performance; 2) In interference-limited scenarios, the performance of traditional RISs is the tight upper bound of STAR-RISs. The numerical results have shown that: 1) The employment of RISs significantly enhances the system coverage, and NOMA schemes improve the rate performance; 2) in low SNR regions, a specific range of energy splitting coefficients guarantees STAR-RISs outperform traditional RISs while in high SNR regions, traditional RISs always have superior performance; 3) STAR-RISs provide flexibility of SIC order in NOMA systems by altering energy splitting coefficients.

APPENDIX A: PROOF OF LEMMA 2

Based on Campbell's theorem, the Laplace transform of the interference for the typical UE can be expressed as follows

$$\begin{aligned}
& \mathcal{L}_{I_r}(s) \\
&= \mathbb{E}_{\Phi_B} \left[\underbrace{\prod_{m \in \Phi_B^T \setminus i} \mathbb{E}_{|h_r|^2} \left[\exp \left(-s\beta^T P_B L_{0,m}^{(k)} |h_r|^2 \right) \right]}_{\text{Transmissive Interference}} \right] \mathbb{E}_{\Phi_B} \left[\underbrace{\prod_{m \in \Phi_B^R \setminus i} \mathbb{E}_{|h_r|^2} \left[\exp \left(-s\beta^R P_B L_{0,m}^{(k)} |h_r|^2 \right) \right]}_{\text{Reflective Interference}} \right] \\
&\stackrel{(a)}{=} \prod_{\chi \in \{T,R\}} \exp \left(-\pi \lambda_B \int_{r_t}^{\infty} \left(1 - \mathbb{E}_{|\tilde{h}_r|^2} \left[\exp \left(-s k_r \theta_r C_r \beta^\chi P_B (r d_t)^{-\alpha_r} |\tilde{h}_r|^2 \right) \right] \right) r dr \right) \\
&\stackrel{(b)}{=} \prod_{\chi \in \{T,R\}} \exp \left(-\pi \lambda_B \int_{r_t}^{\infty} \left(1 - (1 + s \theta_r C_r \beta^\chi P_B (r d_t)^{-\alpha_r})^{-k_r} \right) r dr \right), \tag{A.1}
\end{aligned}$$

where $|\tilde{h}_r|^2 \sim \Gamma(k_r, \frac{1}{k_r})$. (a) is obtained by using the probability generating functional (PGFL) and the fact that $\Gamma(k_r, \theta_r) = k_r \theta_r \Gamma(k_r, \frac{1}{k_r})$. (b) follows from the moment generation function of the Gamma distribution. By applying [26, eq. C.2] in our previous work, we can obtain a more elegant form as shown in (20).

APPENDIX B: PROOF OF THEOREM 1

We denote $Z = \tau_t^* \frac{I_r + n_0^2}{\theta_r \beta^\chi P_B L_{0,i}^{(k)}}$. Based on the fact that $\frac{1}{\theta_r} |h_r|^2 \stackrel{appr.}{\sim} \Gamma(\bar{k}_r, 1)$ as well as the CDF of the Gamma random variable, we have

$$P_{cov,t}^\chi \Big|_{d_{0,i}^{(k)}} = \mathbb{E}_{I_r} \left[e^{-Z} \sum_{m=0}^{\bar{k}_r-1} \frac{Z^m}{m!} \right] = \sum_{m=0}^{\bar{k}_r-1} \frac{(-1)^m}{m!} \left[\frac{\partial^m}{\partial x^m} \mathbb{E}_{I_r} [e^{-Zx}] \right]_{x=1}. \quad (\text{B.1})$$

When the signal transmission mode of assisted STAR-RIS for the typical UE is χ , the coverage probability is expressed as

$$P_{cov,t}^\chi = \int_0^\infty \int_0^\infty \sum_{m=0}^{\bar{k}_r-1} \frac{(-1)^m}{m!} \left[\frac{\partial^m}{\partial x^m} \mathcal{L}_{I_r}(s_\chi x) \exp(-s_\chi n_0^2 x) \right]_{x=1} f_{BR}(r_1) f_{RU}(r_2) dr_1 dr_2, \quad (\text{B.2})$$

where $s_\chi = \frac{\tau_t^*(r_1 r_2)^{\alpha_r}}{\theta_r \beta^\chi P_B C_r}$.

For simplicity, We denote $D_\chi^T = \frac{\tau_t^* \beta^T}{\beta^\chi}$ and $D_\chi^R = \frac{\tau_t^* \beta^R}{\beta^\chi}$. Then we plug (4) and (20) into (B.2).

After some simple algebraic manipulations, the coverage probability is derived as

$$P_{cov,t}^\chi = \int_0^\infty \int_0^\infty 2\pi \lambda_B r_1 f_{RU}(r_2) \sum_{m=0}^{\bar{k}_r-1} \frac{(-1)^m}{m!} \left[\frac{\partial^m}{\partial x^m} \exp(V_\chi(x)) \right]_{x=1} dr_1 dr_2, \quad (\text{B.3})$$

where

$$V_\chi(x) = -s_\chi n_0^2 x - \frac{1}{2} \pi \lambda_B r_1^2 \xi_0(k_r, \alpha_r, D_\chi^T; x) - \frac{1}{2} \pi \lambda_B r_1^2 \xi_0(k_r, \alpha_r, D_\chi^R; x). \quad (\text{B.4})$$

Now let we focus on the high-order derivatives of the composite function $\exp(V(x))$. According to Faà di Bruno's formula [38], we have

$$\begin{aligned} \frac{\partial^m}{\partial x^m} \exp(V(x)) &= \sum_{l=0}^m \exp(V_\chi(x))^{(l)} \mathcal{B}_{m,l} (V_\chi^{(1)}(x), \dots, V_\chi^{(m-l+1)}(x)) \\ &\stackrel{(a)}{=} \exp(V_\chi(x)) \mathcal{B}_m (V_\chi^{(1)}(x), \dots, V_\chi^{(m)}(x)), \end{aligned} \quad (\text{B.5})$$

where $\mathcal{B}_m(x_1, \dots, x_m)$ is the m th complete Bell polynomial. $\mathcal{B}_{m,l}(x_1, \dots, x_{m-l+1})$ is the incomplete Bell polynomial. (a) is obtained by combining the fact that $\exp(x)^{(m)} = \exp(x)$ and the property that $\mathcal{B}_m(x_1, \dots, x_m) = \sum_{l=1}^m \mathcal{B}_{m,l}(x_1, \dots, x_{m-l+1})$.

By applying [39, eq. 15.5.2], the m th derivative of $V(x)$ has the following closed form

$$V_{\chi}^{(m)}(x) = -\Delta^{(m)} - \frac{1}{2}\pi\lambda_B r_1^2 \xi_m(k_r, \alpha_r, D_{\chi}^T; x) - \frac{1}{2}\pi\lambda_B r_1^2 \xi_m(k_r, \alpha_r, D_{\chi}^R; x), \quad (\text{B.6})$$

where $\Delta^{(0)} = s_{\chi} n_0^2 x$, $\Delta^{(1)} = s_{\chi} n_0^2$, and $\Delta^{(m)} = 0$ when $m \geq 2$.

According to the location relationship among the typical UE, the assisted STAR-RIS, and the serving BS, if the STAR-RIS aided link is transmissive, the BS can be only located in the half part of the considered plane \mathbb{R}^2 split by the STAR-RIS and vice versa. Therefore, the overall coverage probability of the typical UE is expressed as

$$P_{cov,t} = \frac{1}{2}P_{cov,t}^T + \frac{1}{2}P_{cov,t}^R. \quad (\text{B.7})$$

Then, the proof is completed.

APPENDIX C: PROOF OF COROLLARY 2

Let we denote $\beta = \beta^T = 1 - \beta^R$. By substituting $s_{\chi} = \frac{\tau_t^*(r_1 r_2)^{\alpha_r}}{\theta_r \beta^{\chi} P_B C_r}$ into (B.4), $V_{\chi}(x)$ can be rewritten as

$$V_{\chi}(x; \beta) = -\frac{c_0 x}{\beta^{\chi}} - \frac{1}{2}\pi r_1^2 \lambda_B \xi_0\left(k_r, \alpha_r, \tau_t^* x; \frac{\beta}{\beta^{\chi}}\right) - \frac{1}{2}\pi r_1^2 \lambda_B \xi_0\left(k_r, \alpha_r, \tau_t^* x; \frac{(1-\beta)}{\beta^{\chi}}\right), \quad (\text{C.1})$$

where $c_0 = \frac{\tau_t^*(r_1 r_2)^{\alpha_r} n_0^2}{\theta_r P_B C_r}$.

To find the optimal energy splitting coefficient for the coverage probability, we take the derivative of $P_{cov,t}$ with respect to β

$$\begin{aligned} \frac{\partial}{\partial \beta} P_{cov,t} &= \frac{\partial}{\partial \beta} \int_0^\infty \int_0^\infty \pi \lambda_B r_1 f_{RU}(r_2) \sum_{m=0}^{k_r-1} \frac{(-1)^m}{m!} \left[\frac{\partial^m}{\partial x^m} \exp(V_T(x; \beta) + V_R(x; \beta)) \right]_{x=1} dr_1 dr_2 \\ &\stackrel{(a)}{=} \int_0^\infty \int_0^\infty \pi \lambda_B r_1 f_{RU}(r_2) \sum_{m=0}^{k_r-1} \frac{(-1)^m}{m!} \left[\frac{\partial^m}{\partial x^m} \frac{\partial}{\partial \beta} \exp(V_T(x; \beta) + V_R(x; \beta)) \right]_{x=1} dr_1 dr_2. \end{aligned} \quad (\text{C.2})$$

where (a) utilize the fact that the high-order derivatives of $\exp(V_{\chi}(x; \beta))$ is continuous, hence the operators of different partial derivatives are interchangeable.

Now let we calculate the first derivative in (C.2), we have

$$\begin{aligned} \frac{\partial}{\partial \beta} \exp(V_T(x; \beta) + V_R(x; \beta)) &\triangleq \frac{\partial}{\partial \beta} \exp(V(x; \beta)) = \exp(V(x; \beta)) \mathcal{B}_1(V^{(1)}(x; \beta)) \\ &= \exp(V(x; \beta)) \left(-c_0 x \left(\frac{1}{(1-\beta)^2} - \frac{1}{\beta^2} \right) \right. \\ &\quad \left. + \frac{\pi r_1^2 \lambda_B}{\beta^2} \xi_1\left(k_r, \alpha_r, \tau_t^* x; \frac{1-\beta}{\beta}\right) - \frac{\pi r_1^2 \lambda_B}{(1-\beta)^2} \xi_1\left(k_r, \alpha_r, \tau_t^* x; \frac{\beta}{1-\beta}\right) \right). \end{aligned} \quad (\text{C.3})$$

It can be easily observed that when $\beta = \frac{1}{2}$, $\frac{\partial}{\partial \beta} P_{cov,t} = 0$. Moreover, when $\beta \rightarrow \frac{1}{2}^-$, $\frac{\partial}{\partial \beta} P_{cov,t} > 0$, and when $\beta \rightarrow \frac{1}{2}^+$, $\frac{\partial}{\partial \beta} P_{cov,t} < 0$. Thus, $P_{cov,t}$ is maximized when $\beta^T = \beta^R = \frac{1}{2}$.

APPENDIX D: PROOF OF THEOREM 3

If $\gamma_{t \rightarrow c} > \tau_c$ holds, we have $\gamma_t > a_t \tau_c^*$. Therefore, (37) can be rewritten as follows

$$\begin{aligned} R_t &= \int_{z > a_t \tau_c^*} \log_2 (1 + \gamma_t) \mathbb{P}(\gamma_t = z) dz \\ &= \int_{z > a_t \tau_c^*} \log_2 (1 + \gamma_t) \frac{\partial}{\partial z} (1 - \mathbb{P}(\gamma_t > z)) dz \end{aligned} \quad (\text{D.1})$$

We denote $\bar{F}_t(z) = \mathbb{P}(\gamma_t > z)$, which represents the CCDF of the decoding SINR for the typical UE. Then (D.1) can be expressed as

$$\begin{aligned} R_t &= - \int_{a_t \tau_c^*}^{\infty} \log_2 (1 + z) \frac{\partial}{\partial z} \bar{F}_t(z) dz \\ &= - \int_{a_t \tau_c^*}^{\infty} \int_0^z \frac{1}{\ln 2(1+x)} dx \frac{\partial}{\partial z} \bar{F}_t(z) dz \\ &\stackrel{(a)}{=} - \frac{1}{\ln 2} \int_0^{a_t \tau_c^*} \frac{1}{1+x} \int_{a_t \tau_c^*}^{\infty} \frac{\partial}{\partial z} \bar{F}_t(z) dz dx - \frac{1}{\ln 2} \int_{a_t \tau_c^*}^{\infty} \frac{1}{1+x} \int_x^{\infty} \frac{\partial}{\partial z} \bar{F}_t(z) dz dx \\ &\stackrel{(b)}{=} \log_2 (1 + a_t \tau_c^*) \bar{F}_t(a_t \tau_c^*) + \frac{1}{\ln 2} \int_{a_t \tau_c^*}^{\infty} \frac{\bar{F}_t(x)}{1+x} dx, \end{aligned} \quad (\text{D.2})$$

where (a) is obtained by exchanging the order of integration. (b) is obtained by using the fact that $\lim_{z \rightarrow \infty} \bar{F}_t(z) = 0$.

Now we calculate $\bar{F}(z)$. Based on (8), we have

$$\bar{F}_t(z) = \frac{1}{2} \sum_{\chi \in \{\text{T}, \text{R}\}} \int_0^{\infty} \int_0^{\infty} \mathbb{P} \left(|h_r|^2 > \frac{(I_r + n_0^2) z}{a_t \beta^{\chi} P_B C_r (r_1 r_2)^{-\alpha_r}} \right) dr_1 dr_2. \quad (\text{D.3})$$

By utilizing the same proof as Theorem 1, we can obtain (38). This proof is completed.

REFERENCES

- [1] P. Yang, Y. Xiao, M. Xiao, and S. Li, “6G wireless communications: Vision and potential techniques,” *IEEE Netw.*, vol. 33, no. 4, pp. 70–75, 2019.
- [2] C. Huang, A. Zappone, G. C. Alexandropoulos, M. Debbah, and C. Yuen, “Reconfigurable intelligent surfaces for energy efficiency in wireless communication,” *IEEE Trans. Wireless Commun.*, vol. 18, no. 8, pp. 4157–4170, 2019.
- [3] M. Di Renzo, A. Zappone, M. Debbah, M. S. Alouini, C. Yuen, J. de Rosny, and S. Tretyakov, “Smart radio environments empowered by reconfigurable intelligent surfaces: How it works, state of research, and the road ahead,” *IEEE J. Sel. Areas Commun.*, vol. 38, no. 11, pp. 2450–2525, 2020.

- [4] Q. Wu and R. Zhang, "Towards smart and reconfigurable environment: Intelligent reflecting surface aided wireless network," *IEEE Commun. Mag.*, vol. 58, no. 1, pp. 106–112, 2020.
- [5] Q. Wu, S. Zhang, B. Zheng, C. You, and R. Zhang, "Intelligent reflecting surface aided wireless communications: A tutorial," *IEEE Trans. Commun.*, pp. 1–1, 2021.
- [6] Y. Liu, X. Liu, X. Mu, T. Hou, J. Xu, M. Di Renzo, and N. Al-Dhahir, "Reconfigurable intelligent surfaces: Principles and opportunities," *IEEE Commun. Surv. Tuts.*, pp. 1–1, 2021.
- [7] Y. Liu, X. Mu, J. Xu, R. Schober, Y. Hao, H. V. Poor, and L. Hanzo, "STAR: Simultaneous Transmission And Reflection for 360° Coverage by Intelligent Surfaces," *arXiv e-prints*, p. arXiv:2103.09104, Mar. 2021.
- [8] X. Mu, Y. Liu, L. Guo, J. Lin, and R. Schober, "Simultaneously Transmitting And Reflecting (STAR) RIS Aided Wireless Communications," *arXiv e-prints*, p. arXiv:2104.01421, Apr. 2021.
- [9] H. Zhang, S. Zeng, B. Di, Y. Tan, M. Di Renzo, M. Debbah, L. Song, Z. Han, and H. V. Poor, "Intelligent Omni-Surfaces for Full-Dimensional Wireless Communications: Principle, Technology, and Implementation," *arXiv e-prints*, p. arXiv:2104.12313, Apr. 2021.
- [10] Z. Ding, Z. Yang, P. Fan, and H. V. Poor, "On the performance of non-orthogonal multiple access in 5G systems with randomly deployed users," *IEEE Signal Process. Lett.*, vol. 21, no. 12, pp. 1501–1505, 2014.
- [11] L. Dai, B. Wang, Y. Yuan, S. Han, I. Chih-lin, and Z. Wang, "Non-orthogonal multiple access for 5G: solutions, challenges, opportunities, and future research trends," *IEEE Commun. Mag.*, vol. 53, no. 9, pp. 74–81, 2015.
- [12] S. M. R. Islam, N. Avazov, O. A. Dobre, and K. Kwak, "Power-domain non-orthogonal multiple access (NOMA) in 5G systems: Potentials and challenges," *IEEE Commun. Surv. Tuts.*, vol. 19, no. 2, pp. 721–742, 2017.
- [13] Ö. Özdogan, E. Björnson, and E. G. Larsson, "Intelligent reflecting surfaces: Physics, propagation, and pathloss modeling," *IEEE Wireless Commun. Lett.*, vol. 9, no. 5, pp. 581–585, 2020.
- [14] W. Tang, M. Z. Chen, X. Chen, J. Y. Dai, Y. Han, M. Di Renzo, Y. Zeng, S. Jin, Q. Cheng, and T. J. Cui, "Wireless communications with reconfigurable intelligent surface: Path loss modeling and experimental measurement," *IEEE Trans. Wireless Commun.*, vol. 20, no. 1, pp. 421–439, 2021.
- [15] S. Zeng, H. Zhang, B. Di, Y. Tan, Z. Han, H. V. Poor, and L. Song, "Reconfigurable intelligent surfaces in 6G: Reflective, transmissive, or both?" *IEEE Commun. Lett.*, vol. 25, no. 6, pp. 2063–2067, 2021.
- [16] J. Lyu and R. Zhang, "Spatial throughput characterization for intelligent reflecting surface aided multiuser system," *IEEE Wireless Commun. Lett.*, vol. 9, no. 6, pp. 834–838, 2020.
- [17] J. Xu, Y. Liu, X. Mu, and O. A. Dobre., "STAR-RISs: Simultaneous transmitting and reflecting reconfigurable intelligent surfaces," *IEEE Commun. Lett.*, pp. 1–1, 2021.
- [18] C. Zhang, W. Yi, Y. Liu, Z. Ding, and L. Song, "STAR-IOS Aided NOMA Networks: Channel Model Approximation and Performance Analysis," *arXiv e-prints*, p. arXiv:2107.01543, Jul. 2021.
- [19] H. Ibrahim, H. Tabassum, and U. T. Nguyen, "Exact coverage analysis of intelligent reflecting surfaces with nakagami-m channels," *IEEE Trans. Veh. Technol.*, vol. 70, no. 1, pp. 1072–1076, 2021.
- [20] C. Pan, H. Ren, K. Wang, W. Xu, M. Elkashlan, A. Nallanathan, and L. Hanzo, "Multicell mimo communications relying on intelligent reflecting surfaces," *IEEE Trans. Wireless Commun.*, vol. 19, no. 8, pp. 5218–5233, 2020.
- [21] H. Xie, J. Xu, and Y.-F. Liu, "Max-Min Fairness in IRS-Aided Multi-Cell MISO Systems with Joint Transmit and Reflective Beamforming," *arXiv e-prints*, p. arXiv:2003.00906, Feb. 2020.
- [22] W. Mei and R. Zhang, "Joint base station-IRS-user association in multi-IRS-aided wireless network," in *IEEE Proc. of Global Commun. Conf. (GLOBECOM)*, 2020, pp. 1–6.

- [23] Z. Zhang and L. Dai, "Capacity improvement in wideband reconfigurable intelligent surface-aided cell-free network," in *Proc. IEEE 21th Int. Workshop Signal Process. Adv. Wireless Commun. (SPAWC)*, 2020, pp. 1–5.
- [24] J. Lyu and R. Zhang, "Hybrid active/pассив wireless network aided by intelligent reflecting surface: System modeling and performance analysis," *IEEE Trans. Wireless Commun.*, pp. 1–1, 2021.
- [25] C. Zhang, W. Yi, and Y. Liu, "Reconfigurable Intelligent Surfaces Aided Multi-Cell NOMA Networks: A Stochastic Geometry Model," *arXiv e-prints*, p. arXiv:2008.08457, Aug. 2020.
- [26] Z. Xie, W. Yi, X. Wu, Y. Liu, and A. Nallanathan, "Modeling and Coverage Analysis for RIS-aided NOMA Transmissions in Heterogeneous Networks," *arXiv e-prints*, p. arXiv:2104.13182, Apr. 2021.
- [27] M. Di Renzo, F. Habibi Danufane, X. Xi, J. de Rosny, and S. Tretyakov, "Analytical modeling of the path-loss for reconfigurable intelligent surfaces – anomalous mirror or scatterer ?" in *Proc. IEEE 21th Int. Workshop Signal Process. Adv. Wireless Commun. (SPAWC)*, 2020, pp. 1–5.
- [28] S. Zeng, H. Zhang, B. Di, Z. Han, and L. Song, "Reconfigurable intelligent surface (RIS) assisted wireless coverage extension: RIS orientation and location optimization," *IEEE Commun. Lett.*, vol. 25, no. 1, pp. 269–273, 2021.
- [29] Y. Xiu, J. Zhao, W. Sun, M. Di Renzo, G. Gui, Z. Zhang, N. Wei, and N. Wei, "Reconfigurable intelligent surfaces aided mmwave NOMA: Joint power allocation, phase shifts, and hybrid beamforming optimization," *IEEE Trans. Wireless Commun.*, pp. 1–1, 2021.
- [30] X. Xie, F. Fang, and Z. Ding, "Joint optimization of beamforming, phase-shifting and power allocation in a multi-cluster IRS-NOMA network," *IEEE Trans. Veh. Technol.*, pp. 1–1, 2021.
- [31] M. Fu, Y. Zhou, Y. Shi, and K. B. Letaief, "Reconfigurable intelligent surface empowered downlink non-orthogonal multiple access," *IEEE Trans. Commun.*, vol. 69, no. 6, pp. 3802–3817, 2021.
- [32] T. Hou, Y. Liu, Z. Song, X. Sun, Y. Chen, and L. Hanzo, "Reconfigurable intelligent surface aided NOMA networks," *IEEE J. Sel. Areas Commun.*, vol. 38, no. 11, pp. 2575–2588, 2020.
- [33] M. Elhattab, M.-A. Arfaoui, C. Assi, and A. Ghayeb, "Reconfigurable intelligent surface assisted coordinated multipoint in downlink NOMA networks," *IEEE Commun. Lett.*, vol. 25, no. 2, pp. 632–636, 2021.
- [34] J. Zuo, Y. Liu, Z. Ding, L. Song, and H. V. Poor, "Joint Design for Simultaneously Transmitting And Reflecting (STAR) RIS Assisted NOMA Systems," *arXiv e-prints*, p. arXiv:2106.03001, Jun. 2021.
- [35] W. Ni, Y. Liu, Y. C. Eldar, Z. Yang, and H. Tian, "STAR-RIS Enabled Heterogeneous Networks: Ubiquitous NOMA Communication and Pervasive Federated Learning," *arXiv e-prints*, p. arXiv:2106.08592, Jun. 2021.
- [36] H. Alzer, "On some inequalities for the incomplete gamma function," *Math. Comput.*, vol. 66, no. 218, pp. 771–778, 1997.
- [37] M. Di Renzo and P. Guan, "Stochastic geometry modeling of coverage and rate of cellular networks using the Gil-Pelaez inversion theorem," *IEEE Commun. Lett.*, vol. 18, no. 9, pp. 1575–1578, 2014.
- [38] K. Cho, J. Lee, and C. G. Kang, "Stochastic geometry-based coverage and rate analysis under nakagami & log-normal composite fading channel for downlink cellular networks," *IEEE Commun. Lett.*, vol. 21, no. 6, pp. 1437–1440, 2017.
- [39] F. Olver, D. Lozier, R. Boisvert, and C. Clark, *The NIST Handbook of Mathematical Functions*. New York, USA: Cambridge Univ. Press, 2010.